International Journal of Heat and Mass Transfer 123 (2018) 89–96

Contents lists available at ScienceDirect

International Journal of Heat and Mass Transfer

journal homepage: www.elsevier.com/locate/ijhmt

Experimental and numerical modeling of heat transfer in directed thermoplates

Imane Khalil *, Ryan Hayes, Quinn Pratt, Christopher Spitler, Daniel Codd

Shiley-Marcos School of Engineering, 5998 Alaclá Park, University of San Diego, San Diego, CA 92110, United States

ARTICLE INFO

Article history:
Received 12 December 2017
Received in revised form 21 February 2018
Accepted 22 February 2018

Keywords:
FLUENT
Computational fluid dynamics
Heat exchanger
Dimpleplate
Experiment validation
Reynolds number

ABSTRACT

We present three-dimensional numerical simulations to quantify the design specifications of a directed thermoplate expanded channel heat exchanger, also called dimpleplate. Parametric thermofluidic simulations were performed independently varying the number of spot welds, the diameter of the spot welds, and the thickness of the fluid channel within the laminar flow regime. Results from computational fluid dynamics simulations show an improvement in heat transfer is achieved under a variety of conditions: when the thermoplate has a relatively large cross-sectional area normal to the flow, a ratio of spot weld spacing to channel length of 0.2, and a ratio of the spot weld diameter with respect to channel width of 0.3. Experimental results performed to validate the model are also presented.

1. Introduction

Thermoplates are efficient heat transfer devices used in a variety of engineering practices. While many methods for manufacturing thermoplates have existed for some time, only recently have computational methods been used to diagnose the often complex flow present inside such devices [1–3]. Garg and Maji, and others have modeled the fluid flow and heat transfer sinusoidal channels with complex velocity fields, flow separation and re-attachments [4–8]. Thermoplate devices with regular, yet non-sinusoidal, spot welds are excellent candidates for parametric analysis using computational fluid dynamics simulations given their complex geometry-dependant flow structure.

The subject of this study is a thermoplate comprised of two sheets of Inconel 625 seam-welded together, with a pattern of spot welds distributed along the fluid direction as shown in Fig. 1. The space between the sheets is hydraulically expanded to a known thickness using a parallel plate guide fixture. The device uses a single fluid, in the liquid phase. This particular heat exchanger is a prototype test-section of a larger design intended for use in a specialized concentrated solar power receiver [9]. This application requires a compact, formable profile with high operating efficiency and minimal temperature gradient between the irradiated wall and heat transfer fluid. Preliminary designs utilize water as the working fluid, with laminar flowrates from 0.5 to 5.0 g/s, pressures ranging from 1 to 50 bar, and outlet temperatures of 80–250 °C.

As opposed to standard thermoplates which often fill an entire sheet with one or more fluids, we consider a directed flow through a single channel. The presence of periodic spot welds, and the complex curvature created during the inflation procedure result in flow structures which undermine the application of analytic solutions.

We present a case-study for this particular breed of thermoplate by varying critical components of the geometry such as the height of the channel, denoted δ, the diameter of the spatially-periodic spot welds, denoted D_s, and the spacing between subsequent spot welds, given by d_s.

For fully developed laminar flow inside ducts, Nu is constant and relatively low. Hence there are large wall-fluid temperature differences, ΔT, between the outer wall and the fluid [10]. The motivation for our work is to enhance the heat transfer by increasing Nu.

First, we present details of the FLUENT Computational Fluid Dynamics (CFD) model used in this study, then we discuss the experiments performed to validate the FLUENT model, followed by the results from independently varying geometric parameters, and concluding with a discussion of the potential for an improved design.

2. Modeling

In this section we address the specifics of developing the model for the thermoplate. First we discuss the theory behind the flow

* Corresponding author.
E-mail address: ikhalil@sandiego.edu (I. Khalil).

https://doi.org/10.1016/j.ijheatmasstransfer.2018.02.093
0017-9310/

Nomenclature

δ	channel height (mm)		
l	channel length (mm)	Re	Reynolds number (based on D_H)
w	channel width (mm)	Nu	Nusselt number
D_s	spot weld diameter (mm)	P	pressure (Pa)
d_s	spot weld spacing (mm)	v	velocity (cm/s)
D_H	hydraulic diameter (mm)	T	temperature (°C)
$\bar{h}$	average heat transfer coefficient (W/m^2·°C)		

inside the thermoplate. We then address the construction of the thermoplate model using the commercial software packages SolidWorks (2016) and ANSYS-FLUENT (17.0) [11]. Due to the complexity of the part, the thermoplate geometry was constructed using the SolidWorks sheet-metal tools and then exported to the ANSYS environment for meshing, and finally FLUENT is used for thermofluidic calculation.

2.1. Theory

The thermoplate in question uses water in the liquid phase as the working fluid. The FLUENT setup included the pressure-based solver with the energy and incompressible laminar flow models. Therefore, the following equations are used in the FLUENT solver:

The continuity equation,

$$\frac{\partial \rho}{\partial t} + \nabla \cdot (\rho \vec{U}) = 0, \tag{1}$$

the momentum equation,

$$\frac{\partial}{\partial t}(\rho \vec{U}) + \nabla \cdot (\rho \vec{U}\vec{U}) = -\nabla P + \nabla \cdot (\bar{\bar{\tau}}) + \rho \vec{g}, \tag{2}$$

the total energy equation,

$$\frac{\partial}{\partial t}(\rho E) + \nabla \cdot (\vec{U}(\rho E + \rho)) = \nabla \cdot \left(k \nabla T - h\vec{J} + (\bar{\bar{\tau}} \cdot \vec{U})\right), \tag{3}$$

where

$$E = h - \frac{P}{\rho} + \frac{U^2}{2}, \tag{4}$$

and enthalpy for incompressible flow is

$$h = \int_{T_{\text{ref}}}^{T} C_p dT + \frac{P}{\rho}, \tag{5}$$

Furthermore, Reynolds number is calculated,

$$Re = \frac{4\dot{m}}{\pi D_H \mu}. \tag{6}$$

In the equations above t is time, ρ is density, $\vec{U}$ is velocity, P is pressure, k is the thermal conductivity, $\vec{J}$ is the diffusion flux, T is temperature and $T_{\text{ref}} = 298.15$ K, $\bar{\bar{\tau}}$ is the stress tensor, C_p is the specific heat, μ is viscosity, and $\dot{m}$ is the mass flowrate.

The performance of the heat exchanger is calculated based on the temperature drop between the inlet and outlet. The performance is evaluated after varying the channel height, δ, the spot weld diameter, D_s, and the weld spacing, d_s. The changes in geometry are generalized with the following ratios,

$$\text{Length Ratio} = \frac{d_s}{l} \quad \text{and} \quad \text{Width Ratio} = \frac{D_s}{w}. \tag{7}$$

Furthermore, the average hydraulic diameter, D_H, is calculated in SolidWorks. The details of the model geometry are discussed in the following section.

Only the fluid inside the channel is present for CFD simulation. The Inconel sheet is represented by a wall boundary condition. Furthermore, because the sheets are inflated from the mid-plane, we can apply a symmetry boundary-condition on the bottom face of the model, as shown in Fig. 3. Thus, the FLUENT model consists of only half of the fluid-domain.

The spots themselves are not modeled as they are part of the Inconel wall, and have no direct-contact with the fluid. Although

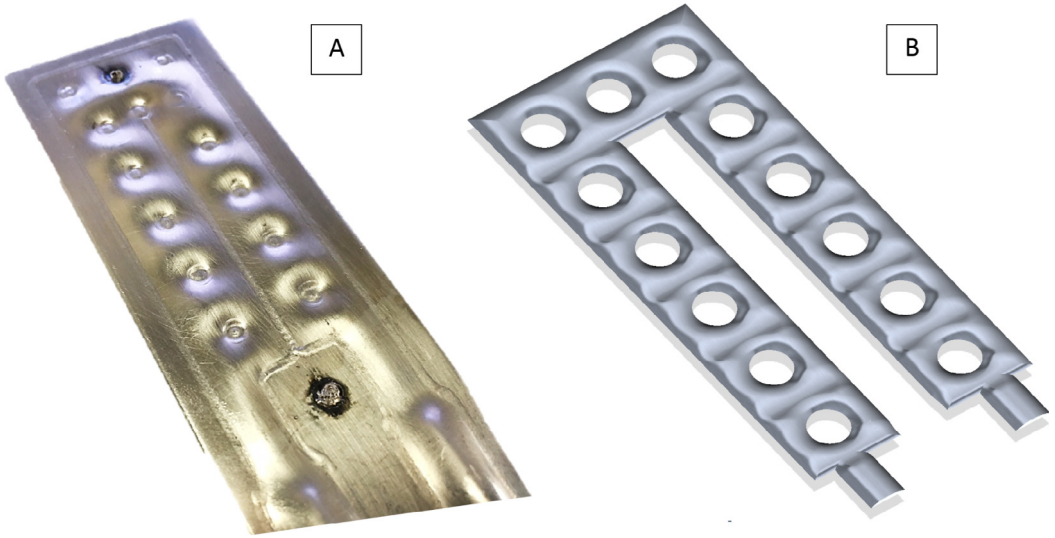

Fig. 1. Figure (A) shows the actual thermoplate used in experiments, the dark marks on the surface are weld locations of thermocouples and should be ignored. Figure (B) shows the SolidWorks model created to validate CFD simulations.

they do participate in the overall heat transfer, it has been shown to have a negligible effect [1]. The boundary conditions were set to achieve an accurate, convergent model. The inlet is set as a 'mass-flow-inlet' in FLUENT and the outlet is set using an 'outflow' condition. The inlet mass flowrate and the inlet temperature are prescribed. The remaining boundary is given a convective boundary condition to treat the interaction between the fluid and the Inconel shell.

With these model considerations, residuals of energy and continuity reach steady-state values after 5000 iterations.

2.2. Geometry and mesh

The construction of a thermoplate typically involves inflating two plates of welded sheet metal. In the present case, the prototype thermoplate was constructed by inflating seam-welded sheets of Inconel 625 to form fluid channels with interspersed spot welds. This process leads to complex surface-curvature which is expected to influence the fluid flow inside the channel, enhance mixing, and improve heat transfer. This curvature also makes modeling the geometry more difficult.

We began with the construction of a highly geometrically-accurate model based on the actual thermoplate used in validation experiments. The actual thermoplate has nominal geometric properties: $l = 47.35$ mm, $w = 8.9$ mm, $\delta = 0.8$ mm, $D_s = 3.7$ mm, and $d_s = 7.6$ mm. After validation, many of the subtleties of the curvature were removed to make further simulations less intensive. While exploring variations in the channel thickness and the spot diameter/spacing, separate SolidWorks models were created. It is important to note that although the geometry was changed several times, the mesh controls and boundary conditions were held constant.

Fig. 1(A, B) compare the actual thermoplate to the geometrically-accurate model created in SolidWorks.

Fig. 2 shows a simplification of the thermoplate to provide labels for our variable parameters used in this study.

Fig. 3 shows the simplified model inside the FLUENT CFD environment and an enlarged portion of the mesh. The simplifications

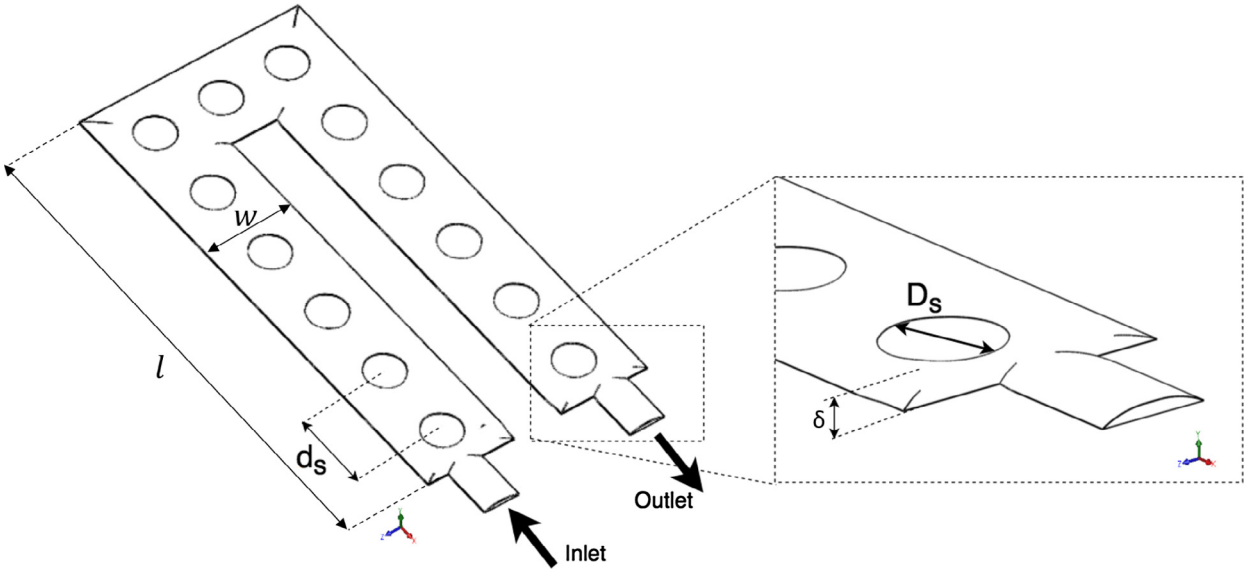

Fig. 2. Schematic drawing showing the inlet and outlet for the water. The channel thickness is δ, the spacing between spot welds is d_s and the diameter of the spot welds is D_s.

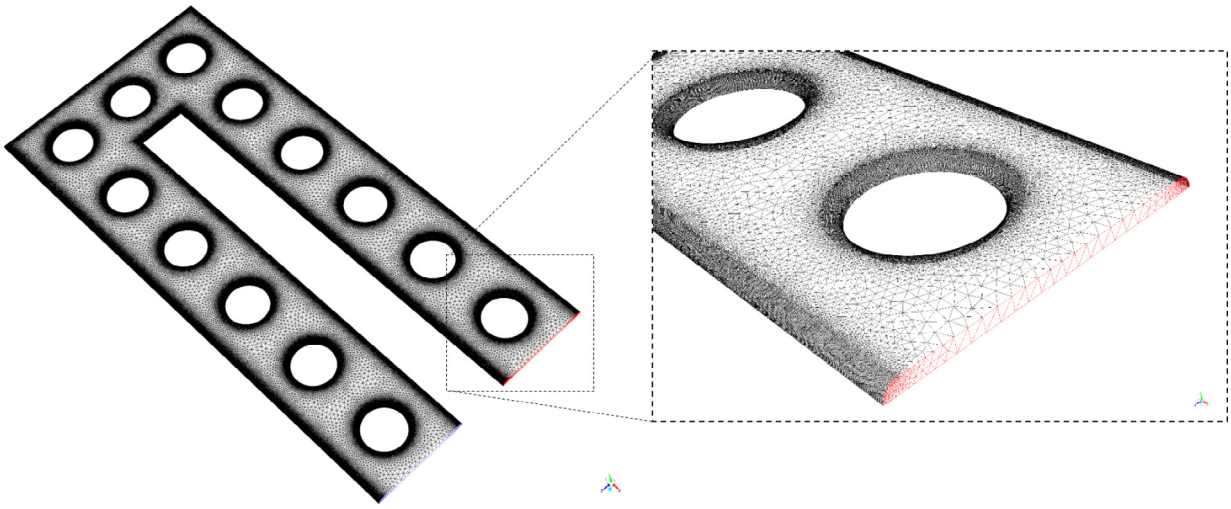

Fig. 3. Simplified CFD mesh using tetrahedral elements. Perspective view of the entire fluid model as well as an enlarged view of the outlet.

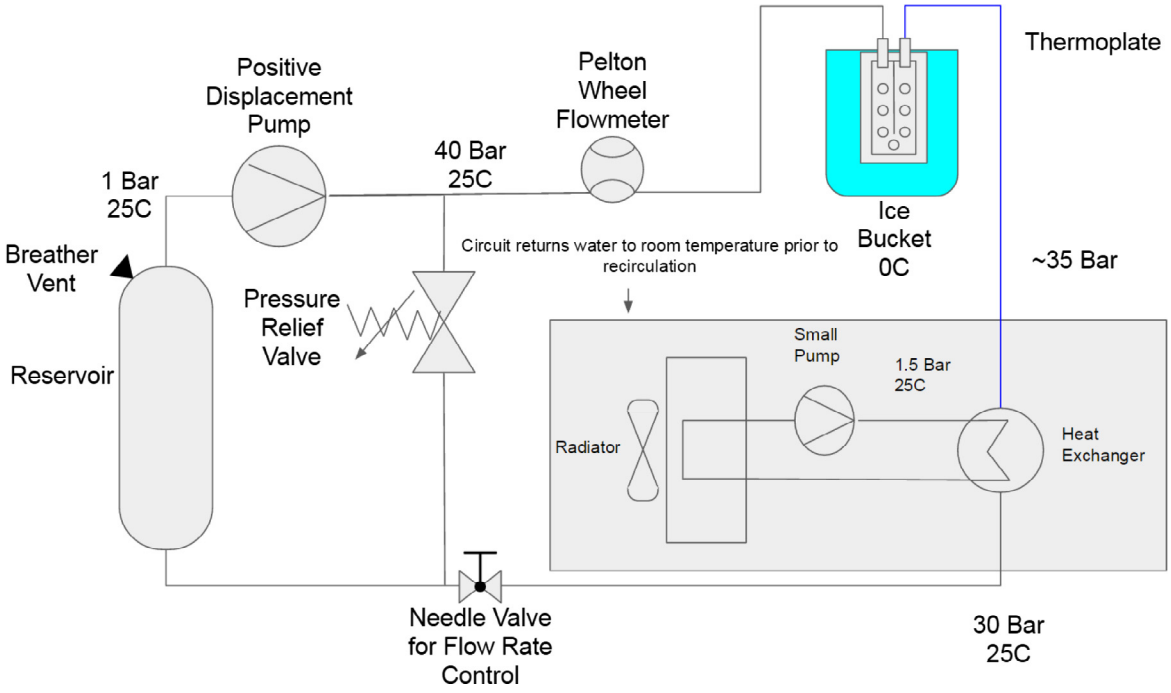

Fig. 4. Diagram of experimental setup. Note that the thermoplate was completely submerged in the ice bath at 0 °C.

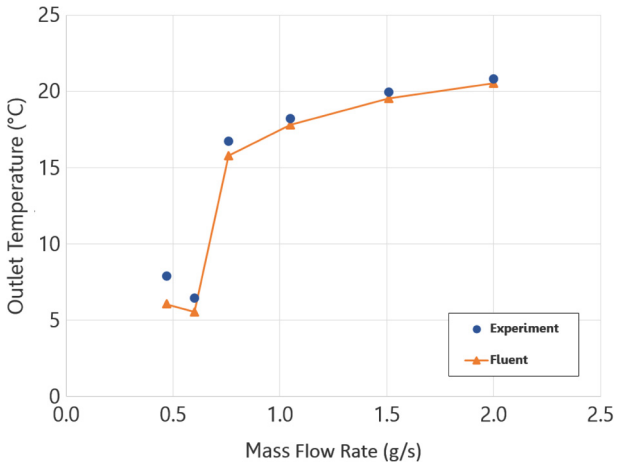

Fig. 5. Comparison of the outlet temperature recorded during experiments with outlet temperatures calculated from FLUENT simulations. Experimental error is ±0.2 °C.

allowed for the model to be reduced from 4 million elements to 1 million. The clock-time on our local machine (Intel Xeon-E3 3.5 GHz, 24 GB RAM) was on the order of four hours.

Although specific mesh statistics vary as we change the geometry, the number of cells remained on the order of 1 million. An adaptive mesh sizing function was used to capture the curvature in close proximity to the spot welds.

3. Experiment

In this section we discuss the experiments used to validate the FLUENT model. The thermoplate used for these experiments was manufactured using the nominal parameters given above, and is shown in Fig. 1(A).

Fig. 4 shows the experimental setup used to calculate the heat transfer coefficient for the thermoplate.

The mass flowrate into the plate is controlled with a positive displacement metering pump with adjustable stroke. For this experiment the stroke length was kept constant and flowrate was adjusted using a needle valve down-stream. The experiment was repeated for the following mass flowrates: 0.47, 0.60, 0.76, 1.05, 1.51, and 2.00 g/s, corresponding to Re = 170, 214, 274, 379, 543, and 717. Flowrate was measured using a model LMX.05 Pelton Wheel Flow Meter manufactured by JLC International specifically for high pressures and low flow. The maximum pressure of fluid entering the thermoplate is set by the pressure relief valve.

During this experiment the pressure relief valve was set to 40 bar. The thermoplate was immersed in an ice bath to induce heat transfer between the working fluid, thermoplate, and surrounding chilled water. The working fluid was recirculated and, in order to keep inlet temperatures constant, a heat control loop is included down-stream of the thermoplate outlet. Heat is exchanged to the secondary loop using a shell and tube heat exchanger and the secondary loop temperature is maintained near room temperature by a fan and radiator. The flow loop system is used in other experiments for testing similar thermoplates heated by solar radiation, where the working fluid reaches a higher temperature and the 40 bar pressure and heat control loop are needed to prevent the water flowing through the thermoplate from undergoing a phase change.

Surface temperatures at two locations on the surface of the plate were collected using type-K thermocouples attached via spot weld (see dark marks in Fig. 1(A)). An average of the two measurements was calculated, denoted T_s. The surface temperature varied while changing the flowrate and was an important measurement for prescribing the boundary conditions of the FLUENT model. Inlet and outlet temperatures were also measured using type-K thermocouples positioned at the center of the flow-path at the location of the tube-fittings.

3.1. Validation of FLUENT model

Simulations were performed using the highly geometrically accurate model with boundary conditions prescribed according to the results from the experiments. The outlet temperature at a

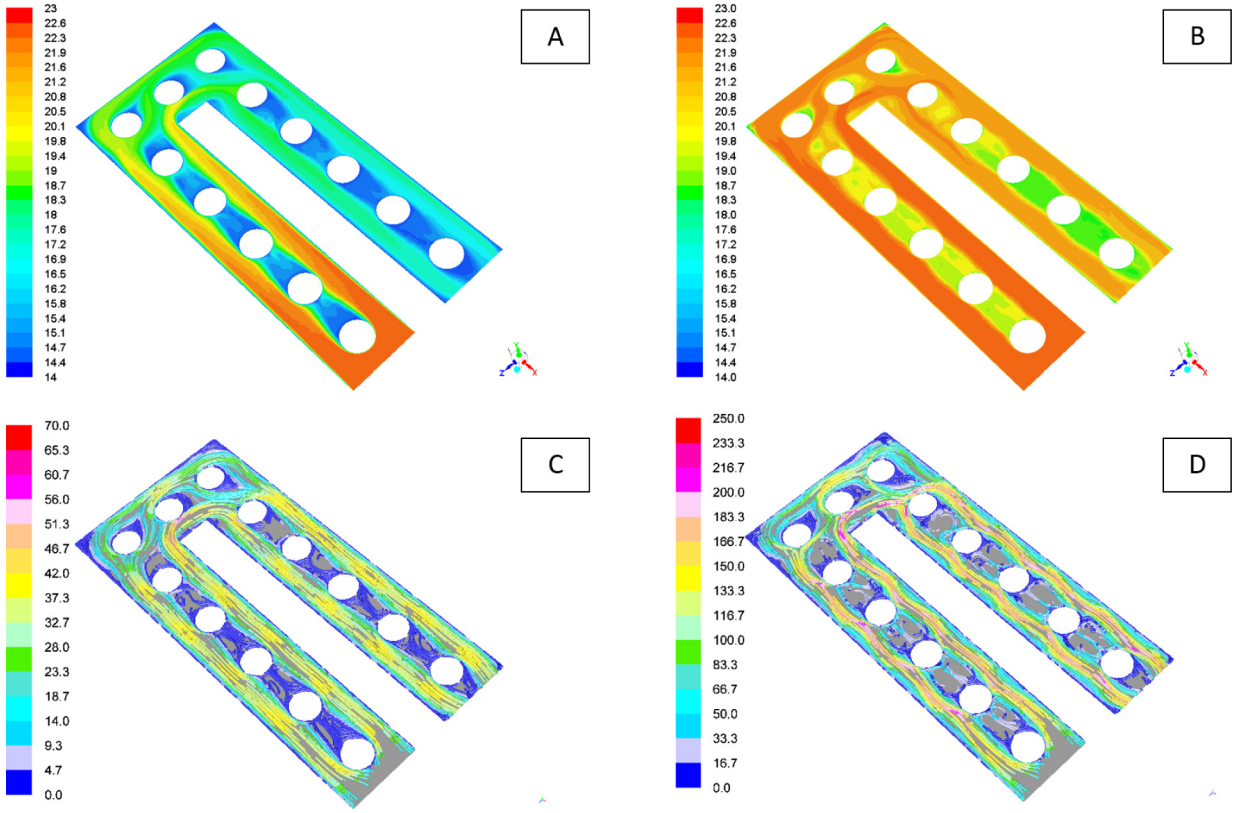

Fig. 6. Result of increasing the flow-rate from 0.5 g/s (A, C) to 2.0 g/s (B, D) on the contours of temperature and the velocity streamlines. Temperatures shown are in degrees Celsius, and velocities are in cm/s.

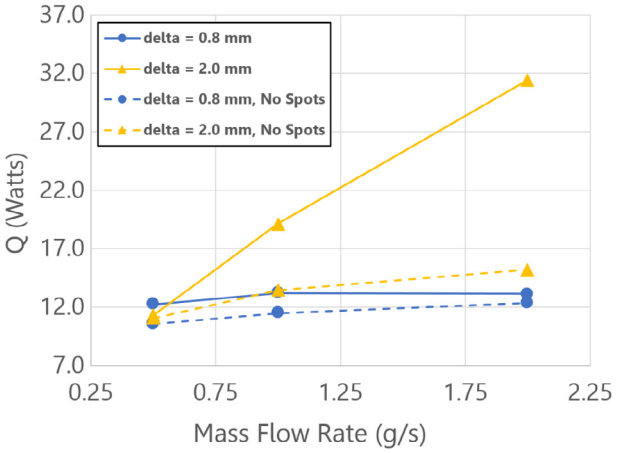

Fig. 7. Heat transferred (Q) as a function of the mass flowrate for a variety of changes to the thermoplate geometry. Shown above are channel heights of $\delta = 0.8$ mm (with and without spot welds) and $\delta = 2.0$ mm (with and without spot welds).

variety of flowrates was recorded in the experiment. Corresponding simulations were performed where the average outlet facet temperature was recorded.

Fig. 5 compares the outlet temperature as a function of mass flowrate for experimental data and FLUENT results. The results appear to be in close agreement thus providing confidence in the ability of our model to capture the subtleties of the real part.

4. Results

After validating the FLUENT model with experimental data, we proceed with exploring the effects of varying the geometry. For the following simulations a simplified model, shown in Fig. 3 was used to reduce the computational complexity.

First we address the results in the simplified model with nominal geometric properties, and the effect of changing the flow-rate. Recall, the nominal geometric properties are: $\delta = 0.8$ mm, $D_s = 3.7$ mm, and $d_s = 7.6$ mm. As we are in the laminar regime, increasing the flowrate resulted in a smaller difference in temperature between the inlet and the outlet. This is due to the fluid being accelerated through the channel without sufficient time to exchange heat. This effect was present in every iteration of the geometry presented, and is therefore omitted from subsequent results.

Fig. 6 demonstrates the effect of increasing the flowrate from 0.5 g/s to 2.0 g/s (Re = 193–816) on the temperature and velocity of the fluid with nominal geometry.

To analyze the effect of varying geometric parameters, new geometry files were created for each case. We will discuss the variation of each parameter accordingly.

4.1. Effect of channel height (δ)

The effect of channel height on the overall heat transfer indicates that the spot welds can dramatically improve the device's ability to remove heat from the working fluid. Fig. 7 gives the relationship between the heat transferred, in Watts, and the mass flowrate through the device. The various trends on the graph illustrate that for a channel thickness δ = 0.8 mm the spot welds lead to a marginal increase in the heat transferred when compared with a thermoplate of equal channel thickness and no spot welds.

However, at the higher flowrate setting of 2.0 g/s (Re = 756) and a thermoplate of thickness $\delta = 2.0$ mm, we see improvement by a factor of nearly 3 over the case without spot welds. This confirms

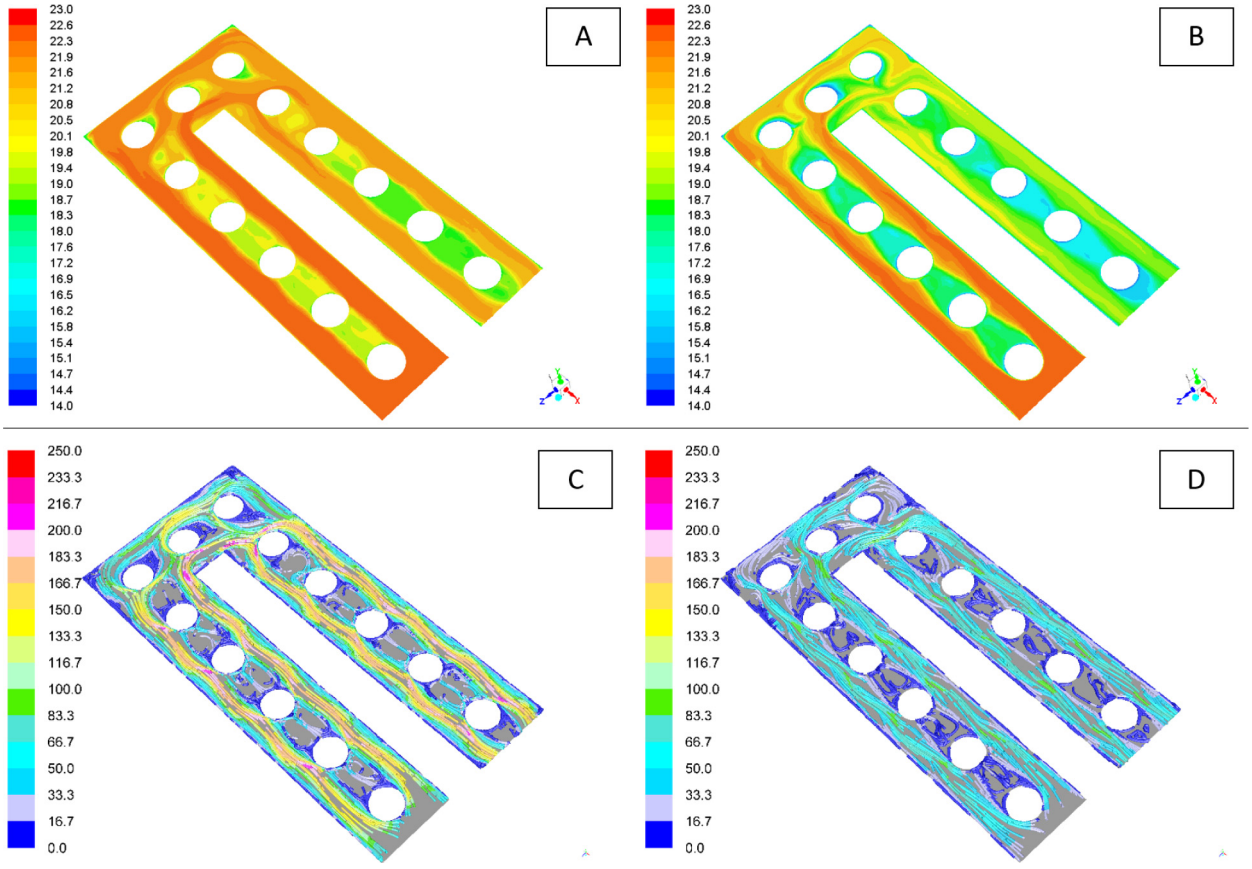

Fig. 8. Figures (A, B) give the contours of temperature (in °C) for a model with $\delta = 0.8$ mm and $\delta = 2.0$ mm for (A) and (B) respectively. Figures (C, D) give velocity streamlines with color corresponding to the velocity magnitude (in cm/s) for $\delta = 0.8$ mm and $\delta = 2.0$ mm for C and D respectively. In each case the flowrate was set to 0.5 g/s. (Re = 145 for a similar-sized channel without spot welds.) (For interpretation of the references to colour in this figure legend, the reader is referred to the web version of this article.)

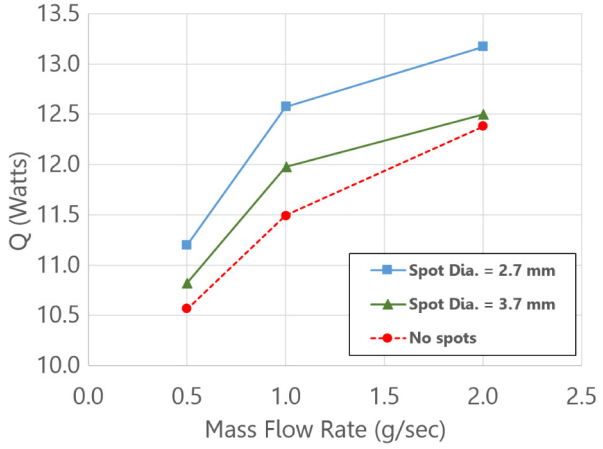

Fig. 9. Effect of changing the diameter of the spot welds, D_s, on the heat transferred, Q, in Watts.

the theory that the spot welds act to induce re-circulation in the flow, hence improving heat transfer.

Fig. 8(A-D) show the CFD results for the cases given in the extremes of Fig. 7. The simulations results indicate that a much higher change in fluid temperature ($\Delta T = T_{out} - T_{in}$) is achieved at constant flowrate with a larger channel. This result is intuitive as the fluid is accelerated through the thermoplate when the channel thickness is decreased at constant flowrate. This conclusion is made clear by the difference in the velocity magnitude shown in Fig. 8(C, D).

4.2. Effect of diameter of welding spot (D_s)

In this section we explore the effect of changing the diameter of the spot welds (D_s) on the thermoplate's ability to transfer heat. Fig. 9 shows the heat transferred (Q) as a function of the mass flowrate for a variety of geometries. The graph in Fig. 9 also includes the results where the thermoplate has no spot welds.

The heat transferred by the thermoplate increases when spot welds are added to the device. However, the heat transferred decreases when the spot weld diameter increases from $D_s = 2.7$ mm to 3.7 mm. This increase and then decrease implies that there is the potential to optimize Q with respect to the spot weld diameter.

Fig. 10 gives the contours of constant temperature throughout the thermoplate for the change in D_s. The difference in the flow structure, seen by proxy through the temperature contours, leads to an interesting conclusion regarding the diameter of the spot weld.

If the spot weld diameter is such that the weld subtends a large fraction of the channel, the flow bifurcates to two parallel channels of decreased hydraulic diameter on either side of the spots (seen in Fig. 10(B)). This dodges the benefits of the spot welds, i.e. their tendency to induce a mixing effect. On the other hand, if the spot weld diameter is selected such that the flow is able to wrap completely around each weld, the fluid maximizes the mixing effect (seen in Fig. 10(A)) and therefore leads to a higher heat transfer.

4.3. Effect of distance between welding spots (d_s)

In this section we address the effect of changing the spacing between subsequent spot welds (d_s) on the surface of the thermo-

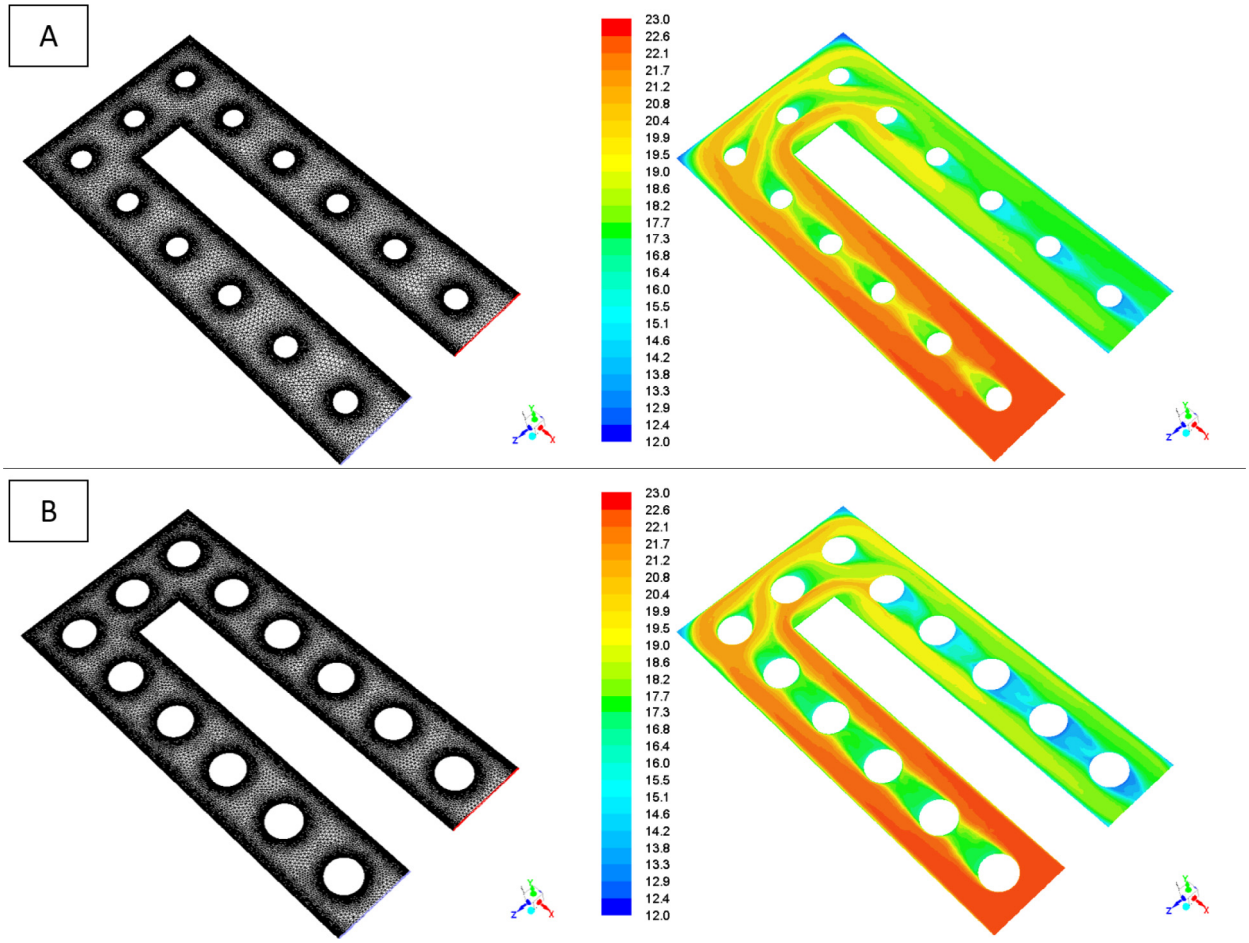

Fig. 10. Figure (A) shows the mesh and temperature contours (in °C) for $D_s = 2.7$ mm. Figure (B) shows the mesh and temperature contours for $D_s = 3.7$ mm. The flow-rate for both cases is 0.5 g/s. (Re = 145 for a similar-sized channel without spot welds.)

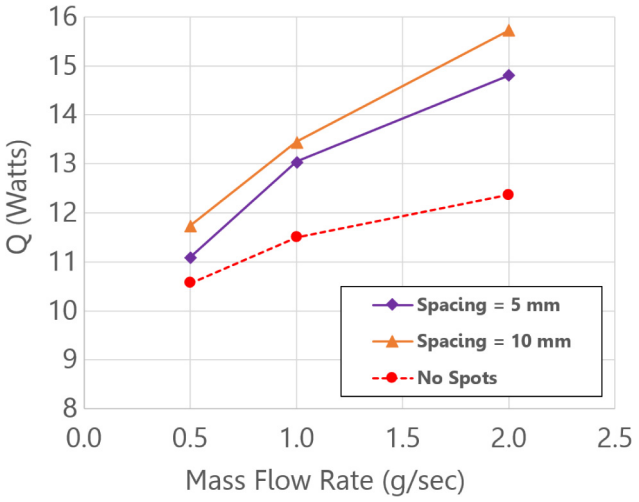

Fig. 11. Effect of changing the spacing between spot welds, d_s, on the total heat transfer, Q, in Watts.

plate. Fig. 11 shows the heat transferred (Q) in Watts as a function of the flowrate for a several geometries, including the geometry containing no spot welds. Similar to the effect of changing the diameter of the spot welds, we observe an increase followed by a subsequent decrease in the heat transferred when transitioning from no spot welds, to a moderate number of spot welds ($d_s = 10$ mm), to a larger number of spot welds ($d_s = 5$ mm).

Fig. 12(A, B) shows a comparison of the geometries as well as contours of constant temperature. Similar to Fig. 10, when the spacing between spots is decreased to a point where the fluid is unable to mix between spot welds there is a decrease in performance. Spacing the spot welds very compactly is another mechanism for reducing the hydraulic diameter of the channel yielding a reduction in the heat transferred.

5. Conclusion

The findings in this report illustrate the complex heat transfer characteristics of a directed thermoplate. The construction of a FLUENT model was validated through experiment. Simulations conducted by individually varying parameters of the geometry were found to suggest the opportunity for improvement.

The improved design characteristics are best represented by the following ratios, calculated using the equations found in Eq. (7): Length Ratio = 0.2, and Width Ratio = 0.3.

Through these simulations we are able to develop an intuition for the performance of this heat exchanger. Our results allowed us to determine an improved design for operation in this domain. The spot welds are found to induce a mixing effect beneficial to heat transfer. However, under certain circumstances related to the aforementioned ratios, when the effective hydraulic diameter decreases we have reduced performance.

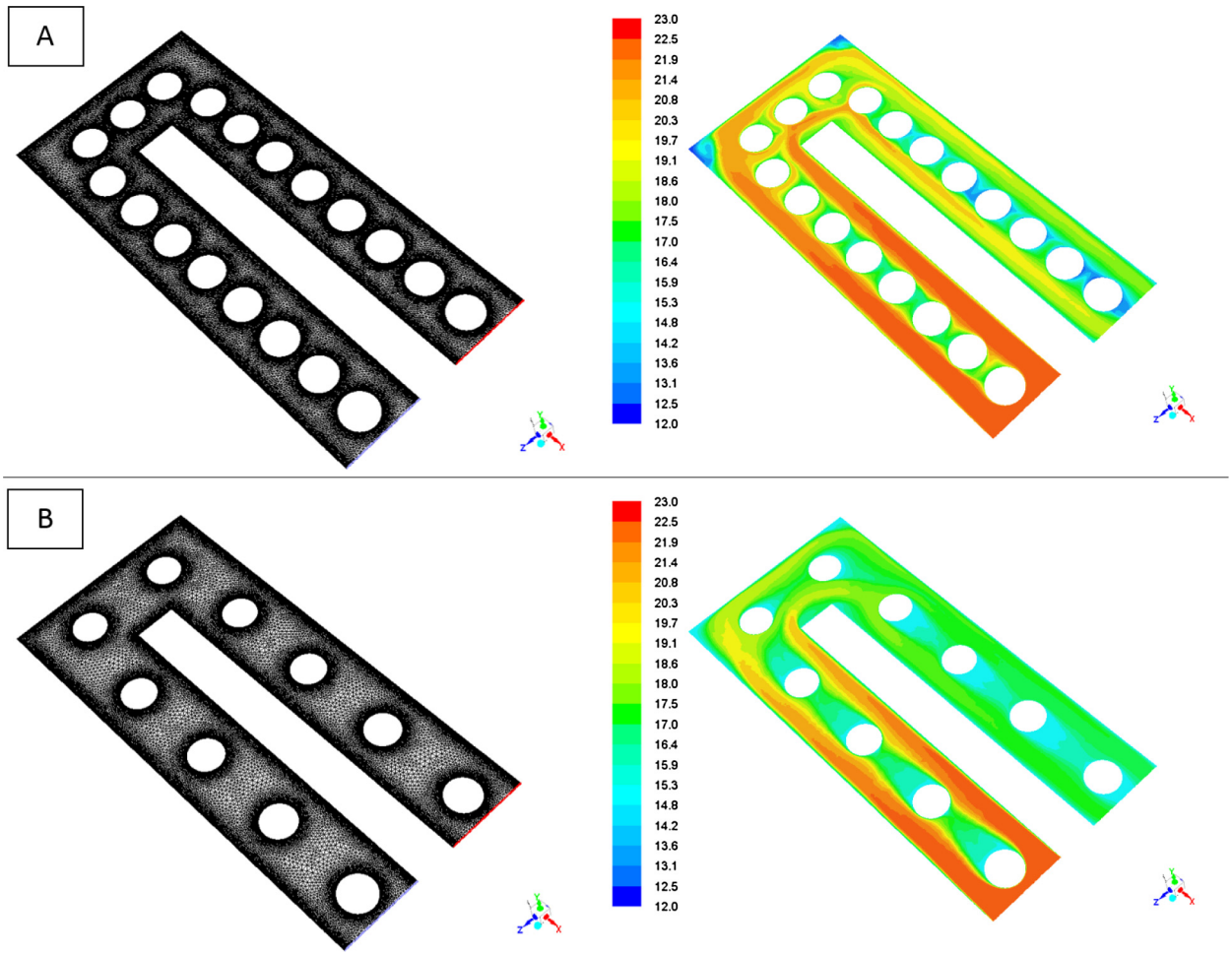

Fig. 12. Figure (A) gives the mesh and temperature contours for a spot weld separation of $d_s = 5.0$ mm. Figure (B) shows the mesh and temperature contours for a spot weld separation of $d_s = 10.0$ mm. The flowrate for each case is 0.5 g/s. (Re = 145 for a similar-sized channel without spot welds.)

6. Future work

Ultimately, this device is a prototype for a three-dimensional formed heat exchanger in development to be used in a concentrated solar power receiver application. The receiver consists of optically heated surfaces with formed flow-paths similar to that of the thermoplate tested in this paper.

Using the conclusions drawn from this paper, the spot weld size and distribution of welds will be adjusted to improve the heat transferred from incoming concentrated sunlight to the working fluid. Future papers will model the formed heat exchanger and optimize the geometric parameters for maximum heat transfer. Optimization tools are available in ANSYS-FLUENT such as the Adjoint Solver. However, these tools require complex constraints and restrict the user's ability to develop an intuition for how the part behaves when varying topological properties, such as the number of holes.

Conflict of interest

The authors declared that there is no conflict of interest.

Acknowledgement

The information, data, or work presented herein was funded in part by the Advanced Research Projects Agency-Energy, U.S. Department of Energy, under Award No. DEAR0000473.

References

[1] J. Mitrovic, B. Maletic, Numerical simulation of fluid flow, heat transfer and pressure drop in thermoplates, HEFAT 2007 (2007).
[2] M. Piper, A. Olenberg, J. Tran, E. Kenig, Determination of the geometric design parameters of pillow-plate heat exchangers, Appl. Therm. Eng. 91 (2015) 1168–1175.
[3] M. Piper, A. Zibart, J. Tran, E. Kenig, Numerical investigation of turbulent forced convection heat transfer in pillow plates, Int. J. Heat Mass Transfer 94 (2016) 516–527.
[4] V.K. Garg, P. Maji, Laminar flow and heat transfer in a periodically converging-diverging channel, Int. J. Numer. Methods Fluids 8 (5) (1988) 579–597.
[5] M.Z. Hossain, A.S. Islam, Fully developed flow structures and heat transfer in sine-shaped wavy channels, Int. Commun. Heat Mass Transfer 31 (6) (2004) 887–896.
[6] G. Russ, H. Beer, Heat transfer and flow field in a pipe with sinusoidal wavy surface—I. Numerical investigation, Int. J. Heat Mass Transfer 40 (5) (1997) 1061–1070.
[7] N. Saniei, S. Dini, Heat transfer characteristics in a wavy-walled channel, J. Heat Transfer 115 (3) (1993) 788–792.
[8] G.v. Wang, S. Vanka, Convective heat transfer in periodic wavy passages, Int. J. Heat Mass Transfer 38 (17) (1995) 3219–3230.
[9] Q. Xu, Y. Ji, B. Riggs, A. Ollanik, N. Farrar-Foley, J.H. Ermer, V. Romanin, P. Lynn, D. Codd, M.D. Escarra, A transmissive, spectrum-splitting concentrating photovoltaic module for hybrid photovoltaic-solar thermal energy conversion, Sol. Energy 137 (2016) 585–593.
[10] T.L. Bergman, Introduction to Heat Transfer, John Wiley & Sons, 2011.
[11] ANSYS, Inc., ANSYS Academic Research User-Manual, 17th ed., 2017.